SIMULTANEOUS RECONSTRUCTION OF ABSORPTION AND SCATTERING DISTRIBUTIONS IN TURBID MEDIA USING A BORN ITERATIVE METHOD

Yuqi Yao*, Yao Wang*, Yaling Pei*, Wenwu Zhu* and Randall L. Barbour+

* Polytechnic University, Brooklyn, NY 11201

+ SUNY Health Science Center, Brooklyn, NY 11203

ABSTRACT

In this paper, we present a Born Iterative Method for imaging optical properties of turbid media using frequency-domain data. In each iteration, the incident field and the associated weight matrix are first recalculated based on the previous reconstructed image. A new estimate is then obtained by solving the updated perturbation equation. The forward solution of the incident field is obtained by a multigrid finite difference method. The inversion is carried out through a Tikhonov regularized optimization process using the conjugate gradient descent. Using this method, the distribution of the complex wavenumbers in a test medium is first reconstructed, from which the absorption and scattering distributions are then derived. Simulation results have shown that this method can yield quantitatively quite accurate reconstruction even when a strong perturbation exists between the actual medium and an assumed homogeneous background medium, in which case the Born approximation cannot work well. Both full-angle and limited angle measurement schemes have been simulated to understand the effect of the location of detectors and sources.

1. INTRODUCTION

Recently, there has been intense interest in the use of frequency domain optical measurement to study the physical phenomena [1-3] and to image objects [4-7] in highly scattering media such as human tissue. Such studies have the prospects of yielding a new diagnostic tool for early detection of tumors in the human body in the near future. The imaging problem entails the reconstruction of the absorption and scattering coefficients in an inhomogeneous scattering medium, from measurements of multiple scattered light signals on the medium surface. This is an inverse scattering problem. This inverse problem is difficult because the scattered field is nonlinearly related to the properties of the medium, and that multiple scattering events occur randomly and cannot be neglected for objects with strong contrasts. These difficulties make it impossible to find a closed-form solution. In the past, either the Born or Rytov approximation has been utilized to linearize the problem. However, such approximation is not valid under strong perturbations, *i.e.,* when the absorption or scattering coefficients of the actual medium are significantly different from those of a chosen background. Our tests have shown that the Born or Rytov approximation fails to yield quantitatively correct reconstruction when the absorption coefficient of an embedded object is three times more of that of the background medium, or when the scattering coefficient is twice more.

A general way to solve the inverse problem is via an iterative approach. Chew et al. used so-called *Born Iterative Method* (BIM) and *Distorted Born Iterative Method* (DBIM) successfully to solve nonlinear 2-D profile inversion for electromagnetic problems using both single-frequency and time domain data [8-10]. In this paper we apply the Born Iterative Method in the optical imaging problem, to solve for the absorption and scattering coefficients of a turbid medium under optical illumination. Starting with a chosen homogeneous background field, the Born approximation is employed to derive a linear perturbation equation, which is then solved to yield the first image. In each of the following iterations, the incident field and the associated weight matrix are first recalculated based on the previous reconstructed image. A new estimate is then obtained by solving the updated perturbation equation. The forward solution of the incident field is

0-8194-1929-X/95/$6.00

obtained by a multigrid finite difference method [11-13]. The inverse solution of the perturbation equation is based on the regularized least squares formulation, obtained by a conjugate gradient descent method [15]. Using this method, the distribution of the complex wavenumbers in a test medium is first reconstructed, from which the absorption and scattering distributions are then derived. The method will be illustrated with simulations performed for test media under different types of perturbations. It is shown that very accurate reconstruction can be achieved via this algorithm, even under strong perturbation. Reconstruction examples from both full-angle and limited angle measurement will be presented.

2. FORMULATION

2.1 Diffusive Light Transport in Turbid Media

Let $\mu_a(\mathbf{r})$ and $\mu_s'(\mathbf{r})$ represent the absorption and equivalent-isotropic scattering coefficients in a medium, respectively, and $D(\mathbf{r}) = [3(\mu_a(\mathbf{r})+\mu_s'(\mathbf{r}))]^{-1}$ represent the diffusion coefficient. In general, these quantities are position-dependent. The frequency domain diffusion equation for the fluence rate $u(\mathbf{r})$, due to a sinusoidally intensity-modulated point source of light, is given by [13]:

$$\nabla^2 u(\mathbf{r}) + k^2(\mathbf{r})u(\mathbf{r}) = -S(\mathbf{r}) - \frac{\nabla D(\mathbf{r}) \cdot \nabla u(\mathbf{r})}{D(\mathbf{r})}, \tag{1}$$

where $k^2(\mathbf{r}) = -\mu_a/D(\mathbf{r}) + i\omega/cD(\mathbf{r})$, is wave number, c is the speed of light in the tissue, $S(\mathbf{r})$ represents the source signal.

Consider the actual medium as a perturbation of a homogeneous background medium with absorption and scattering coefficients described by μ_a^b and $\mu_s^{b'}$, respectively, with an associated diffusion coefficient $D_b = [3(\mu_a^b + \mu_s^{b'}]^{-1}$ and wave number ${k_b}^2 = -\mu_a^b/D_b + i\omega/cD_b$. Let

$$O(\mathbf{r}) = k^2(\mathbf{r}) - {k_b}^2 \tag{2}$$

be the perturbation in terms of the wave number, to be called the object function. From Eq. (1), we can derive the following scalar wave equation:

$$\nabla^2 u(\mathbf{r}) + k_b^2 u(\mathbf{r}) = S(\mathbf{r}) - \mathcal{L}(\mathbf{r})u(\mathbf{r}), \tag{3}$$

where

$$\mathcal{L}(\mathbf{r}) = O(\mathbf{r}) + \frac{\nabla D(\mathbf{r}) \cdot \nabla}{D(\mathbf{r})}. \tag{4}$$

In the paper, we neglect the second term in Eq. (4). The general case in which this term is not neglected will be reported in another paper.

From Eq. (3), it can easily be shown that $u(\mathbf{r})$ satisfies the following nonlinear volume integral equation:

$$u_s(\mathbf{r}) = \int_v G(\mathbf{r}, \mathbf{r}')O(\mathbf{r}')u(\mathbf{r}')d^3\mathbf{r}', \tag{5}$$

where

$$u_s(\mathbf{r}) = u(\mathbf{r}) - u_b(\mathbf{r}) \tag{6}$$

is the scattered field measured at the detector, $u_b(\mathbf{r})$ is the background field (*i.e.,* the total field of the background medium under the same source illumination), and $G(\mathbf{r}, \mathbf{r}')$ is the Green's function of the homogeneous background satisfying:

$$\nabla^2 G(\mathbf{r}, \mathbf{r}') + k_b^2 G(\mathbf{r}, \mathbf{r}') = -\delta(\mathbf{r} - \mathbf{r}'). \tag{7}$$

2.2 The Born Iterative Method for Image Reconstruction

The integral equation in (5) can be discretized to yield a linear system of equations with complex coefficients as follows:

$$\mathbf{W}_{(\mathbf{m}\times\mathbf{n})}\mathbf{o}_{(\mathbf{n})} = \mathbf{u}_{(\mathbf{m})}, \tag{8}$$

where $\mathbf{O} = [O(\mathbf{r}_j), j = 1, 2, \cdots, n]^T$ is composed of the values of $O(\mathbf{r})$ at various voxels $\mathbf{r}_j$; $\mathbf{u} = [u_s(\mathbf{r}_{d_i}, \mathbf{r}_{s_i}), i = 1, 2, \cdots, m]^T$ consists of the scattered field obtained with different source-detector pairs $(\mathbf{r}_{d_i}, \mathbf{r}_{s_i})$; and $\mathbf{W}$ is a weight matrix with elements:

$$W_{ij} = G(\mathbf{r}_{d_i}, \mathbf{r}_j)u(\mathbf{r}_{s_i} - \mathbf{r}_j)\delta v, \quad i = 1, \cdots m, j = 1, \cdots n, \tag{9}$$

where δv is the volume of a voxel. The weight matrix depends on the physics of the problem (such as the properties of the background medium, the Green's function, the total field, and measurement geometry). In the inverse scattering problem, the properties of the medium (*i.e.*, $k(\mathbf{r})$ or equivalently $o(\mathbf{r})$) and consequently the total field $u(\mathbf{r})$ and the weight matrix are unknown. In order to solve Eq. (9), we adopt the following iterative method:

1. Solve the Green's function $G(\cdot, \cdot)$ and background field $u_b(\cdot)$, based on $k_b^2(\cdot)$, using a multigrid finite difference method [13].
2. Let $u(\mathbf{r}) = u_b(\mathbf{r})$, *i.e.*, the Born approximation.
3. Calculate the weight matrix W from the previously calculated total field $u(\cdot)$ and Green's function $G(\cdot, \cdot)$, according to Eq. (9).
4. Solve the perturbation equation in Eq. (8) for the object function $O(\mathbf{r})$ by employing Tikhonov regularization optimization process using the conjugate gradient descent method [14-15].
5. Using the recently found $O(\mathbf{r})$ in a forward scattering problem to solve the total field $u(\mathbf{r})$ inside the object and calculate the scattered field at the detector. In this procedure, a multigrid scheme [13] is employed for all forward calculation.
6. Compare the measured scattered field with that obtained in step 5. If the two quantities are within an acceptable value, stop the iterations. Otherwise, go back to step 3.

Fig. 1 shows a flow chart of this algorithm.

2.3 Simultaneous Reconstruction of Absorption and Scattering Distributions

With frequency domain data, the object function $O(\mathbf{r})$ is a complex function of absorption and scattering distributions. We can find the absorption and scattering coefficients from the real part and imaginary part of the object function. Assume that $\mu_a = \mu_a^b + \delta\mu_a$, $\mu_s' = \mu_s'^b + \delta\mu_s'$. Substituting them into Eq. (2), we obtain:

$$Re[O(\mathbf{r})] = -3(\mu_a^b + \delta\mu_a)(\delta\mu_a + \delta\mu_s') - \frac{\delta\mu_a}{D_b} \tag{10}$$

and

$$Im[O(\mathbf{r})] = \frac{3\omega}{c}(\delta\mu_a + \delta\mu_s') \tag{11}$$

Solving the above two equations, we obtain the absorption and scattering coefficients as follows:

$$\delta\mu_a(\mathbf{r}) = -\frac{\mu_a^b \frac{Im[O(\mathbf{r})]}{\omega/c} + Re[O(\mathbf{r})]}{\frac{Im[O(\mathbf{r})]}{\omega/c} + 3(\mu_a^b + \mu_s'^b)} \tag{12}$$

and

$$\delta\mu_s'(\mathbf{r}) = \frac{\{Re[O(\mathbf{r})] + 3(3\mu_a^b + \mu_s'^b) + \frac{Im[O(\mathbf{r})]}{\omega/c}\}\frac{Im[O(\mathbf{r})]}{3\omega/c}}{\frac{Im[O(\mathbf{r})]}{\omega/c} + 3(\mu_a^b + \mu_s'^b)}. \tag{13}$$

Based on Eqs. (13) and (14), we can derive the perturbations in absorption and scattering distributions easily once the complex object function (*i.e.*, the perturbation in the wave number) is obtained.

3. SIMULATION AND RESULTS

In this section, we show the reconstruction results for cylindrical media containing one or two rods. Both the forward and inverse calculations are done for a 2-D plane of this cylindrical system. The modulation frequency used is 200 MHz. Both full-angle and limited-angle source and detector configurations are simulated. In all the examples, the measured data are calculated by solving the forward scattering problem with the true absorption and scattering distribution functions by using a multigrid finite different method [13].

3.1 Full-Angle Profile Inversion

Consider the geometry depicted in Fig. 2. An unknown object $O(\mathbf{r})$ is embedded in a homogenous background medium with $\mu_a^b = 0.02cm^{-1}$ and $\mu_s'^b = 10.0cm^{-1}$. A total of 10 sources and 20 detectors are located uniformly over a ring of radius 4 cm. The detectors separately collect the signal of the field scattered by the object due to the transmitted field by each source. A rectangular region enclosing the source-detector ring is discretized into 33×33 grid points. The goal is to simultaneously reconstruct the absorption and scattering coefficients at these grid points.

Fig. 3 shows the reconstruction results for a medium containing a rod with a radius of $0.7cm$ at the center of the detector ring. Only perturbation in absorption is simulated in this case. The perturbation is largest at the center, being $0.2cm^{-1}$, and smoothly decreases to zero at the boundary of the rod following a sinusoidal pattern. Fig. 3(a) shows the image of the actual absorption perturbation and Figs. 3(b)-3(c) present the reconstruction results obtained after 1, 10, and 15 iterations. Here, we can see that the one step Born approximation (*i.e.*, one iteration) can reveal the existence of a centered object, but fails to yield an accurate estimate of the spatial range and perturbation magnitude of the object. The reconstruction accuracy improves significantly with more iterations. The solution obtained with 15 iterations is quite close to the true absorption perturbation. Note that the perturbation simulated here is very strong, 10 times of that of the background.

Fig. 4 shows the reconstruction results for a medium containing a rod with a radius of $0.7cm$ at a position $1.5cm$ away from the center. The rod has larger absorption and scattering coefficients than the background. The perturbation follows the same sinusoidal pattern as in the previous example. The peak values of the perturbations in the absorption and scattering coefficients are $0.1cm^{-1}$ and $10.0cm^{-1}$, respectively. Figs. 4(a) and 4(e) show the actual absorption and scattering perturbation distributions, respectively. Simultaneous reconstruction of the absorption and scattering perturbations are attempted. Figs. 4(b)-4(d) are the reconstructed perturbation in absorption obtained after 1, 5, and 10 iterations.

Figs. 4(f)-4(h) present similar results for the perturbation in scattering. Again, it can be seen that the reconstruction result after 10 iterations is quite accurate, with significant improvement in terms of both spatial range and perturbation intensities, compared to the result obtained with one iteration.

Fig. 5 shows the reconstruction results for a medium containing two rods, each rod having the same geometry and optical properties as the one in the previous example. In order to evaluate the effect of noise in data on the reconstruction accuracy, we compare the results from the original calculated data and those subjected to 10% (SNR=20 dB) noise. Here we only show the reconstruction results obtained after 10 iterations. Fig. 5(a) is the actual distribution of the magnitude of the object function (see Eq. (11)). Figs. 5(b) and 5(c) are the reconstructed object functions (magnitude only) from the original and noise added data, respectively. Figs. 5(d)-5(f) present similar results for the perturbation in absorption, while Figs. 5(g)-(i) are for the perturbation in scattering. It can be seen that with this example, the reconstruction results are only accurate qualitatively, correctly identifying the presence of two objects. But the estimated spatial range and perturbation magnitude of the object are not very accurate. With noise-free data, the two rods are located quite accurately with slight blurring, and estimated perturbation magnitudes are approximately half of the actual ones. But with noise-added data, the objects are poorly located (especially for the scattering properties) and the peak perturbation values are severely underestimated. Additional iterations are expected to improve the reconstruction accuracy.

3.2 Limited-Angle Profile Inversion

The full angle measurement schemes used in the previous examples may not be feasible in practice. Here, we consider two types of limited angle measurement schemes. In the circular limited-angle case, shown in Fig. 6(a), 10 sources and 20 detectors are spread uniformly along a semi-circle ranging from -65^0 to 65^0. In the line limited-angle case, shown in Fig. 6(b), 10 sources and 20 detectors are located along a line from $-4cm$ to $4cm$. The test medium is the same as that for the example shown in Fig. 4, containing an off-center rod with perturbations in both absorption and scattering following a sinusoidal pattern.

Figs. 7(a) and 7(b) show the reconstructed absorption and scattering distributions, respectively, from circular limited-angle data. Figs. 7(c) and 7(d) show the reconstruction results from line limited-angle data. In both cases, the results are obtained with 10 iterations. Compared to the results obtained from full-angle data, shown in Figs. 4(d) and 4(h), the peak values of absorption and scattering are estimated less accurately. Among these two types of limited angle measurement schemes, they yield quite similar reconstructions of absorption distributions, but the circular limited-angle case lead to a better reconstruction of the scattering distribution.

4. CONCLUSIONS

A Born iterative method is described for imaging of absorption and scattering distributions in turbid media using frequency domain data. This method has been applied for several test media containing one or two rods with strong perturbations. Reconstructions from full-angle as well as limited-angle measurement data have been attempted. For the case when a single object is embedded in a homogeneous medium, quantitatively accurate reconstruction have been achieved, even when the difference between the optical properties of the object and those of the background is very large. The reconstruction result is substantially improved over that obtained based on the first order Born approximation. The results obtained with limited angle data are less accurate than those from full angles, but still quite useful. However, for a test medium containing two objects, both with strong perturbations, the perturbation magnitudes tend to be under estimated. When the data are corrupted by noise, the reconstruction accuracy is further reduced quantitatively. The reconstruction results obtained here are obtained with 10 to 15 iterations. Future work

will focus on improving the reconstruction accuracy for multiple objects problem. The method could easily be applied to the three-dimensional inverse problem, if computational resources are available.

In the BIM, only the total field are updated based on the previously reconstructed medium. We are currently investigating a distorted Born iterative method in which the Green's function is also updated. This method is expected to reduce the number of iterations required to obtain the same accuracy by the BIM. We hope to report the results of this method soon.

5. REFERENCES

[1] J. Fishkin and E. Gratton, "Propagation of photon-density waves in strongly scattering media containing an absorbing semi-infinite plane bounded by a straight edge," *J. Opt. Soc. Am. A,* 10, 127-140 (1993).

[2] B. J. Tromberg, L.O. Svaasand, T.T. Tsay and R.C. Haskell, "Properties of photon density waves in multiple-scattering media," *Applied Optics,* 32, 607-616 (1993).

[3] Y. Q. Yao, Y. Wang, R. L. Barbour, H. L. Graber and J. W. Chang, "Scattering Characteristics of Photon Density Waves from an Object in a Spherically Two-Layer Medium," *In SPIE Proceedings on Biomedical Optics*, B. Chance and R. R. Alfano, ed., Vol. 2389, pp. 291-303, (1995)

[4] A. Knuttel, J.M. Schmitt and J.R. Knutson, "Spatial localization of absorbing bodies by interfering diffusive photon-density waves," *Applied Optics*, 32, No. 4, 381-389 (1993).

[5] E. Gratton and J. Maier, "Frequency-domain Measurements of Photon Migration in Highly Scattering Media," in *Medical Optical Tomography*, G. Muller, ed., SPIE Institute for Advanced Optical Technologies (SPIE Optical Engineering Press Vol. IS11, 1993), pp. 534-544.

[6] M. A. O'Leary, D.A. Boas, B. Chance and A.G. Yodh, "Imaging of inhomogeneous turbid media using diffuse photon density waves," *In OSA Proceedings on Advances in Optical Imaging and Photon Migration*, R. R. Alfano, ed., pp. 106-115 (1994).

[7] B. W. Pogue and M. S. Patterson, " Forward and Inverse Calculations for Near-Infrared Imaging Using a Multigrid Finite Difference Method," *In OSA Proceedings on Advances in Optical Imaging and Photon Migration*, R. R. Alfano, ed., pp. 176-180 (1994).

[8] Y. M. Wang and W. C. Chew, "An Iterative Solution of the Two-Dimensional Electromagnetic Inverse Scattering Problem," *Int. J. Imaging Syst. Technol.,* vol.1, pp.100-108, (1989).

[9] W. C. Chew and Y. M. Wang, "Reconstruction of Two-dimensional Permittivity Distribution Using The Distorted Born Iterative Method," *IEEE Trans. Medical Imag.,* vol. 9, pp. 218-225, (1990).

[10] M. Moghaddadam and W. C. Chew, "Nonlinear Two-dimensional Velocity Profile Inversion Using Time-Domain Data," *IEEE Trans. Geosi. Remote Sensing,* pp. 146-156, (1992).

[11] R. E. Alcouffe, A. Brandt, J. E. Dendy and J. W. Painter, " The Multi-grid Method for the Diffusion Equation with Strongly Discontinuous Coefficients," *SIAM J. Sci. Stat. Comput.,* 2, pp. 430-454, (1981).

[12] J. C. Adams, "MUDPACK: Multigrid Portable Fortran Software for the Efficient Solution of Linear Elliptic Partial Differential Equation," *Appl. Math. Comp. 34,* pp. 113-146 (1989).

[13] Y. Q. Yao, Y. Wang, Y. L. Pei, W. W. Zhu, J. H. Hu and R. L. Barbour, " Frequency Domain Optical Tomography In Human Tissue," *in this proceedings.*

[14] A. N. Tikhonov and V. Y. Arsenin, *Solution of Ill-posed Problem,* Washington D. C., V. H. Winston, (1977).

[15] W. W. Zhu, Y. Wang, R. L. Barbour, H. L. Graber and J. W. Chang, " Regularized Progressive Expansion Algorithm for Recovery of Scattering Media from Time-Resolved Data," *In OSA Proceedings on Advances in Optical Imaging and Photon Migration*, R. R. Alfano, ed., pp. 211-216, (1994).

ACKNOWLEDGEMENT

This work was supported in part by the National Institutes of Health under Grant # RO1-CA59955, by an ONR grant # N000149510063, and by the New York State Science and Technology Foundation.

THE BORN ITERATIVE METHOD

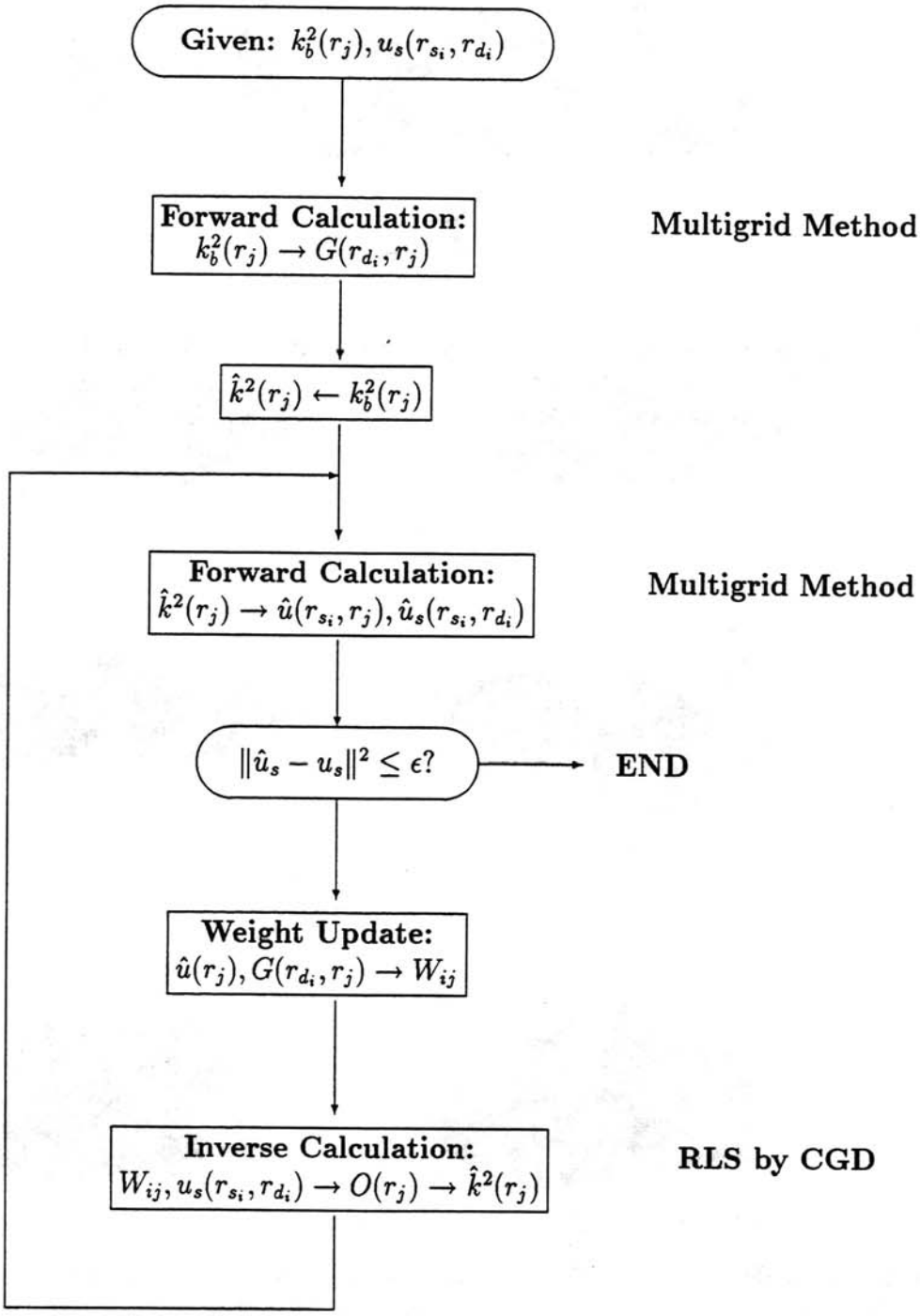

Figure 1: A flow chart of Born iterative algorithm

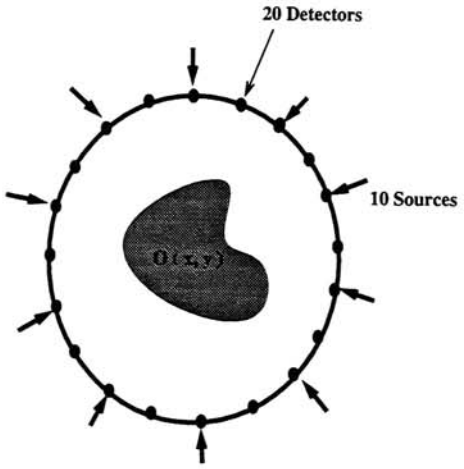

Figure 2: Data acquisition geometry for full-angle profile inversion "S" and "D" denote source and detector, respectively, $O(\mathbf{r})$ is the object function.

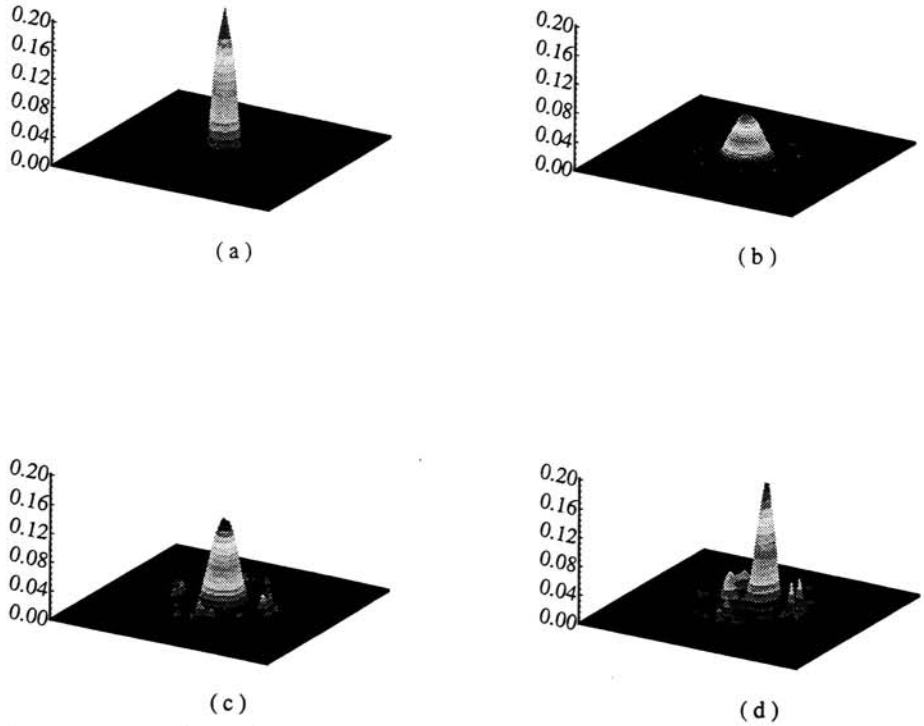

Figure 3: Full-angle reconstruction of a pure absorption perturbation of a medium with a centered rod. The modulation frequency is 200 MHz. The background properties are $\mu_a^b = 0.02cm^{-1}$ and $\mu_s'^b = 10.0cm^{-1}$. The peak value of the absorption perturbation is $0.2cm^{-1}$. (a) is the image of the true perturbation, (b)-(d) are the reconstruction images after 1 iteration (*i.e.*, Born approximation), 10 and 15 iterations.

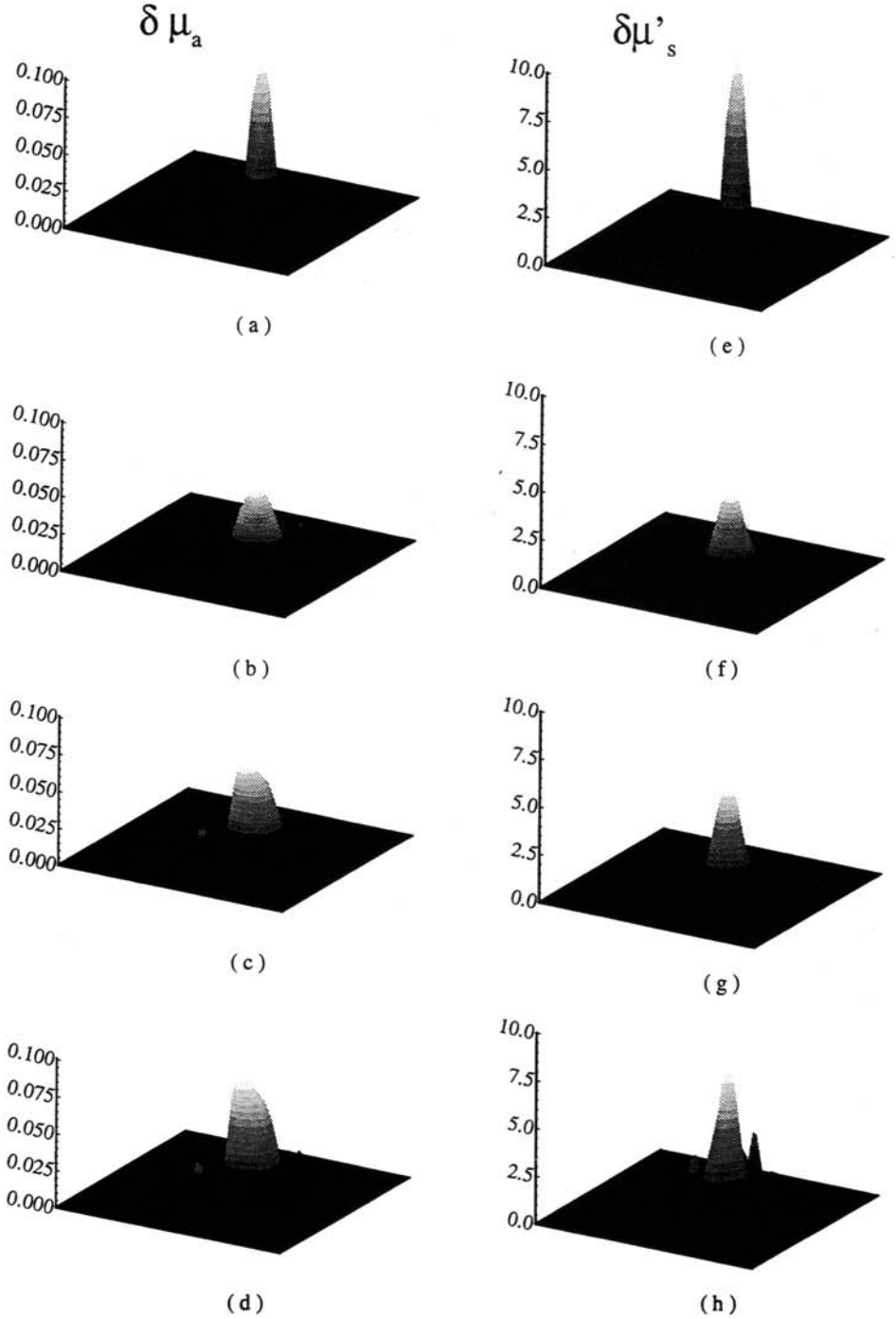

Figure 4: Full-angle simultaneous reconstruction of the absorption and scattering distributions of a medium with an off-center rod at $1.5cm$. The modulation frequency is 200 MHz. The background properties of medium are $\mu_a^b = 0.02cm^{-1}$ and $\mu_s'^b = 10.0cm^{-1}$. The peak values of the absorption and scattering perturbation are respectively $0.1cm^{-1}$ and $10.0cm^{-1}$. (a) is the original absorption perturbation, (b)-(d) are the reconstruction results after 1, 5 and 10 iterations, respectively. (e) is the original scattering perturbation, and (f)-(h) are the reconstruction results after 1, 5 and 10 iterations, respectively.

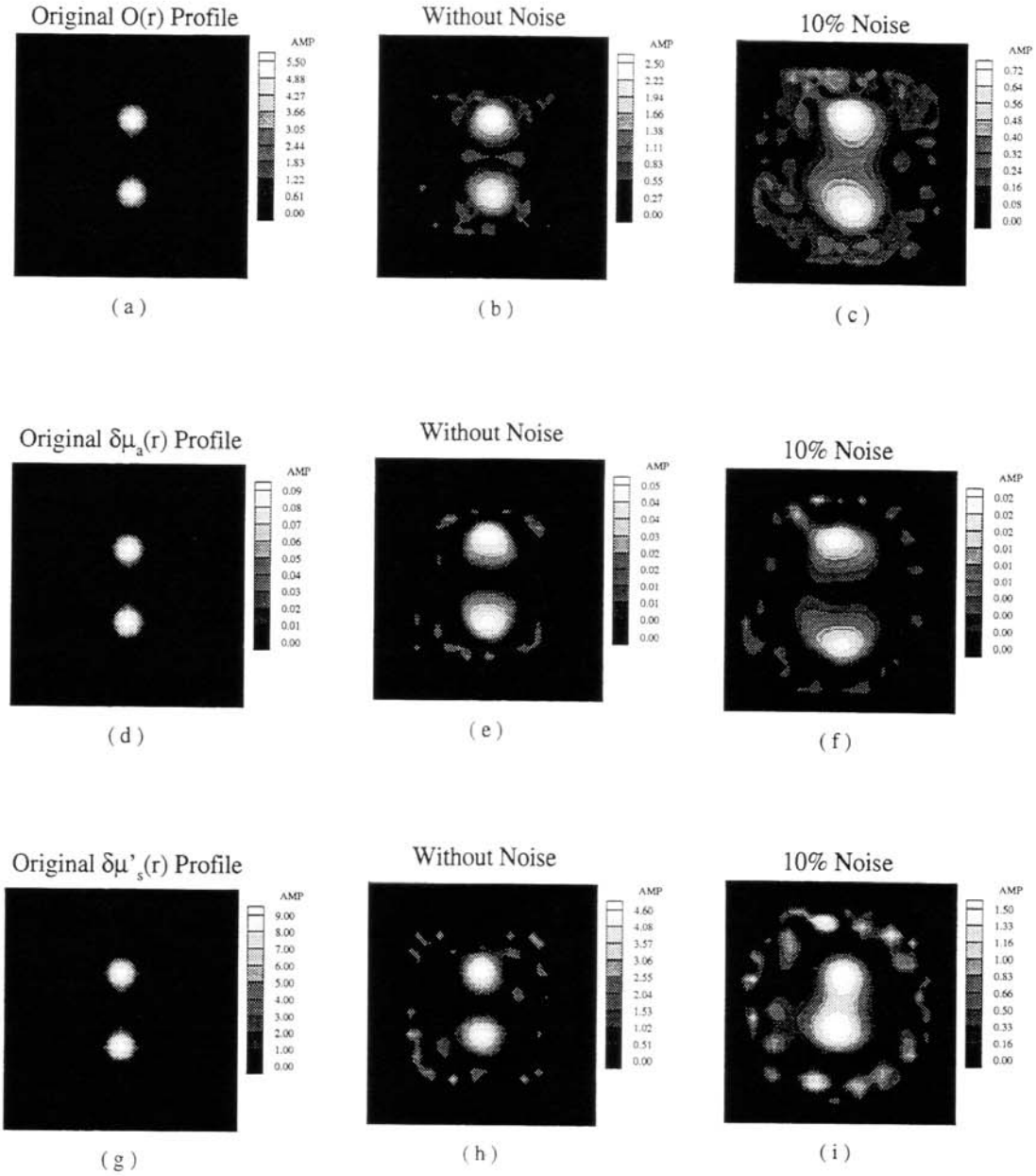

Figure 5: Full-angle reconstruction of the object function as well as absorption and scattering distributions in a medium with two rods separated by $3cm$. The modulation frequency is 200 MHz. The background properties of the medium are $\mu_a^b = 0.02cm^{-1}$ and $\mu_s'^b = 10.0cm^{-1}$. The reconstruction results are obtained with 10 iterations.

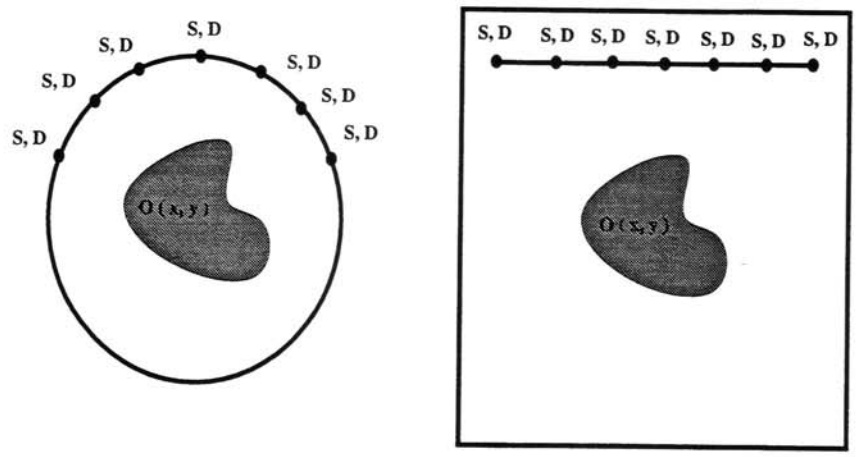

(A) (B)

Figure 6: Data acquisition geometry for (A) Circular limited-angle profile inversion and (B) Line limited-angle profile inversion. In each case 10 sources and 20 detectors are used.

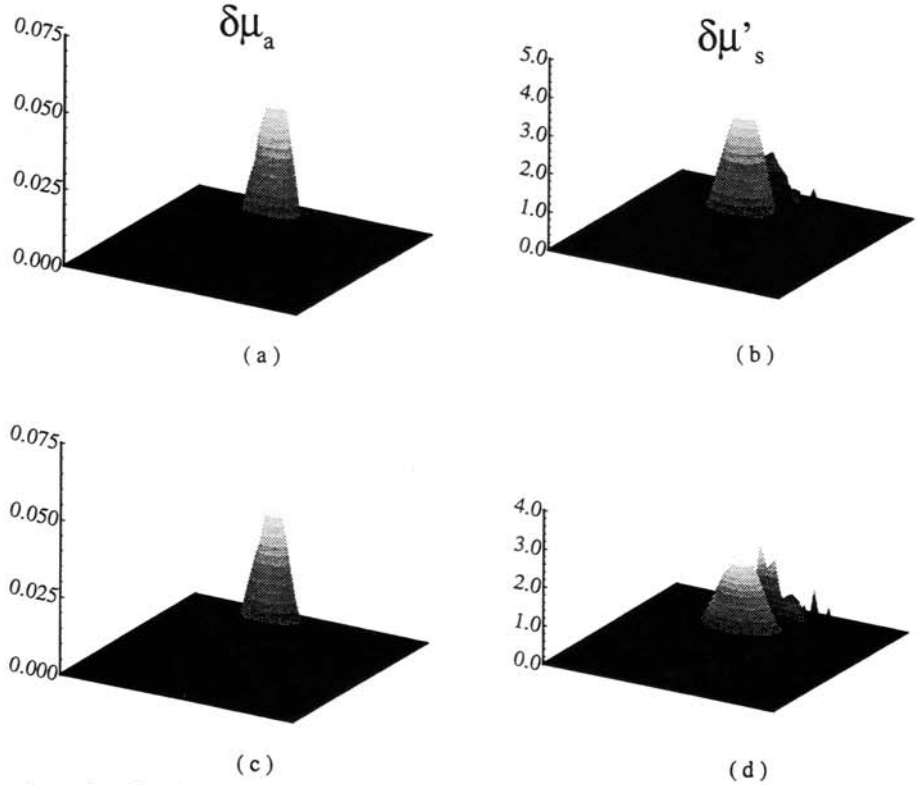

Figure 7: Limited-angle simultaneous reconstruction of the absorption and scattering distribution in a medium with an off-center rod at $1.5cm$ with modulation frequency is 200 MHz. The background properties of the medium are $\mu_a^b = 0.02cm^{-1}$ and $\mu_s'^b = 10.0cm^{-1}$. The original images of the absorption and scattering perturbation are shown in Figs. 3(a) and 3(e). (a) and (b) are reconstruction absorption and scattering distributions obtained with 10 iterations from the circular limited data. (c) and (d) are the reconstruction results obtained with 10 iterations from line limited data.